FPGA CO-DESIGN FOR EFFICIENT N:M SPARSE AND QUANTIZED MODEL INFERENCE

Fen-Yu Hsieh*
Institute of Information Science
Academia Sinica
hsieh0013@as.edu.tw

Yun-Chang Teng*
Institute of Information Science
Academia Sinica
yteng@iis.sinica.edu.tw

Ding-Yong Hong
Institute of Information Science
Academia Sinica
dyhong@iis.sinica.edu.tw

Jan-Jan Wu
Institute of Information Science
Academia Sinica
wuj@iis.sinica.edu.tw

ABSTRACT

Large language models (LLMs) have demonstrated remarkable performance across a wide range of language processing tasks. However, this success comes at the cost of substantial computation and memory requirements, which significantly impedes their deployment in resource-constrained environments. To address this challenge, this work introduces an automation framework that leverages weight pruning and low-bit quantization, and presents a hardware-software co-design method that generates accelerators on the Field-Programmable Gate Array (FPGA) platform. In particular, we implement a unified pipeline that applies N:M structured pruning and 4-bit integer quantization to reduce the memory footprint, followed by optimized dequantization and matrix multiplication to enhance LLM inference on several hardware platforms, including CPUs, NVIDIA GPUs with Dense and 2:4 Sparse Tensor Cores, and a custom systolic-array-based FPGA accelerator. Utilizing 2:4 sparsity combined with quantization on 4096×4096 matrices, our approach achieves a reduction of up to $4\times$ in weight storage and a $1.71\times$ speedup in matrix multiplication, yielding a $1.29\times$ end-to-end latency reduction compared to dense GPU baselines. Scaling analysis on the LLaMA-7B model further shows that structured sparsity enhances the throughput per token by $1.36\times$. These results demonstrate the synergy of fine-grained N:M sparsity and quantization for enabling efficient and deployable LLM inference, while the proposed FPGA accelerator offers a flexible architectural path for supporting a broader class of sparsity patterns beyond the fixed 2:4 hardware constraints.

Keywords Accelerator · FPGA · High-level Synthesis · Weight Pruning · Quantization · Machine Learning

1 Introduction

Large language models (LLMs) [1] have substantially advanced language processing tasks such as natural language understanding and generation [2]. However, their large scale and heavy computational requirements present significant challenges for both deployment and real-time inference [3]. This limitation impedes the realization of pervasive deep learning, which necessitates real-time inference and low energy consumption in resource-constrained environments [4].

*These authors contributed equally to this work and are listed in alphabetical order.

F. Y. Hsieh: conceived the overall compression–acceleration framework, designed the N:M sparsity and quantization pipeline, implemented the CPU and dense/sparse GPU baselines and benchmarking scripts, designed the measurement methodology and LLaMA-7B scaling analysis, and led the writing and revision of the manuscript.

Y. C. Teng: designed the systolic array-based accelerator, architecture of zero-skipping processing elements, bridged software and hardware design by creating a host for workload preprocessing and offloading, and built the HLS flow and FPGA implementation flow for deployment.

Consequently, numerous model compression methods, such as sparsification and quantization, have been developed to reduce the size and complexity of LLMs [5].

Pruning and quantization methods reduce computational and memory overhead by removing redundant weights or lowering numerical precision, enabling smaller and faster models with limited accuracy degradation [6, 7]. However, using either technique alone often provides an incomplete solution. Pruning reduces the number of operations but leaves activations and remaining weights at full precision, while quantization decreases precision but does not reduce the number of computation operations. Therefore, combining the two techniques offers a more comprehensive compression strategy, simultaneously lowering arithmetic cost, memory bandwidth, and model size. This joint approach is particularly important for LLMs, where both weight storage and data movement dominate inference latency and energy consumption [8, 9].

Additionally, a central question to the pruning approaches is how sparsity should be structured. Unstructured pruning can achieve high sparsity, but without specialized hardware or library support, its practical acceleration benefits remain limited [10]. The N:M fine-grained structured sparsity has emerged as a promising solution, with NVIDIA Ampere and subsequent architectures providing dedicated hardware support for the fixed 2:4 pattern. However, current hardware support is often restricted to this fixed 2:4 configuration, despite algorithmic studies suggesting that alternative N:M patterns may yield better accuracy. This mismatch between flexible algorithmic designs and rigid hardware constraints motivates the need for new methods to obtain compact, fast, and deployable LLMs.

To address the aforementioned issues, this work presents a hardware-software co-design methodology that generates FPGA-based accelerators to enable efficient inference of LLMs compressed using both pruning and quantization. Furthermore, we develop a unified framework that automatically performs model compression and supports multiple hardware platforms, including our FPGA-based accelerator, as well as modern processors such as CPUs, NVIDIA GPUs with Dense Tensor Cores, and NVIDIA GPUs with 2:4 Sparse Tensor Cores. Our framework is further distinguished by two key features: The software component is designed to support generalized N:M sparsity patterns ($N < M$) and low-bit precision ($B < 8$ bits) to be applied across LLM weights and activations. The hardware component introduces a systolic-array-based FPGA accelerator architecture specifically engineered for the efficient processing of generalized N:M sparse and B-bit quantized data. This efficiency is realized through a dynamic zero-skipping mechanism and a reconfigurable datapath that accommodates diverse N:M patterns and bit-widths. We further introduce a general analytical model to guide the design space exploration of the optimal N:M patterns and bit-widths, with the objective of maximizing hardware utilization and throughput while minimizing accuracy degradation.

The remainder of this paper is organized as follows. Section 2 reviews background and related work. Section 3 introduces our unified framework, and Section 4 describes the details of our FPGA-based accelerator. Section 5 evaluates our method. Section 6 concludes the paper.

2 Backgrounds and Related Works

Model compression. Neural networks has traditionally relied on weight pruning and quantization to reduce memory footprint and computation cost. Pruning compresses models by removing redundant or unimportant weights that contribute little to the predictive accuracy. Quantization reduces the precision of numerical values such as weights and activations from high-precision formats (e.g., 32-bit floating point) to lower-precision formats (e.g., 8-bit integers). Early work such as Deep Compression [11] demonstrated that magnitude pruning combined with low-bit quantization can substantially shrink model size while preserving accuracy. SpQR [12] proposes a sparse–quantized representation that stores outlier weights separately in higher precision while quantizing the remaining weights to 3-bit or 4-bit, achieving lower perplexity on LLaMA models. SqueezeLLM [13] similarly combines sensitivity-based pruning with non-uniform quantization, obtaining 3-bit LLaMA models with modest accuracy degradation. These approaches highlight the possibility of combining pruning and quantization to achieve smaller models with only limited accuracy loss.

Building on this idea, later work focuses not only on the compressed formats themselves but also on how pruning and quantization interact. JSQ [14] introduces a saliency metric that accounts for both weight magnitude and activation range, enabling balanced selection of surviving weights before quantization. SLiM [2] further integrates quantization, structured sparsity, and low-rank adaptation (LoRA) in a unified one-shot pipeline, showing that 2:4 sparsity with 4-bit weights can still preserve downstream accuracy when combined with LoRA compensation.

In contrast to prior work that optimizes a specific sparse–quantized format, our goal is to generalize model compression with N:M structured sparsity with low-bit quantization under realistic LLM workloads. We adopt magnitude-based N:M pruning, including but not limited to the 2:4 pattern used by NVIDIA sparse tensor cores, and pair it with uniform low-bit quantization.

Systolic Array.

3 Unified Framework

3.1 Designed Pipeline

To address the computation and memory bottlenecks of large language models on resource-constrained hardware, we design a unified pipeline that combines N:M structured pruning with low-bit quantization. While each technique individually reduces model size and arithmetic cost, their combination introduces practical challenges such as sparsity metadata management, dequantization overhead, and platform-dependent implementation details. Our goal is to provide a streamlined, platform-agnostic flow that compresses weights once offline in a consistent format and exposes a common execution interface for CPUs, dense GPUs, NVIDIA 2:4 sparse tensor cores, and FPGA accelerators. This enables fair benchmarking of compressed models and supports hardware/software co-design without modifying the high-level model description for each back-end.

This section presents the component-level pipeline, including the offline weight compression via combining N:M structured pruning with quantization, and the online execution of dequantization and matrix multiplication. Figure 1 illustrates the overall workflow. The pipeline consists of two stages. The offline preparation stage is shown in the green panel, and the online benchmark execution stage is shown in the red panel. During the offline stage, we transform dense FP16 weights into compressed N:M sparse INT4 value tensors and store them with compact metadata and scaling factors. During the online stage, we load these compressed tensors onto the target device, dequantize them back into FP16 values while preserving sparsity, and perform matrix multiplication with FP16 activations through a device-specific GEMM kernel.

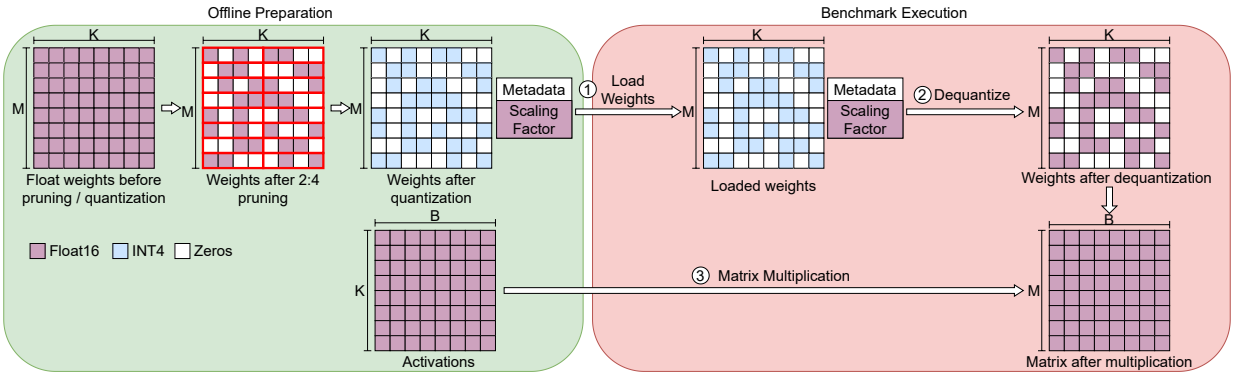

Figure 1: Overview of the proposed pipeline. The green panel shows the offline preparation (N:M pruning, quantization, and packing). The red panel shows the benchmarking path (loading, dequantization, and matrix multiplication) across platforms. Purple cells indicate Half-Precision 16-bit Floating Point (FP16) values, white cells indicate zeros, and blue cells indicate 4-byte integer (INT4) nonzeros.

3.2 Offline Preparation

The offline preparation stage converts dense FP16 weight matrices into a compact sparse–quantized format that can be used efficiently across all hardware back-ends. As illustrated in Figure 2, this stage applies two transformations. First, N:M structured pruning removes low-magnitude weights within fixed-size groups, producing a regular sparsity pattern that preserves the overall matrix shape. Second, the surviving nonzero values are quantized to low-bit integers, reducing storage cost and memory bandwidth. These two steps are performed once prior to deployment, and the resulting compressed weights, scaling factors, and sparsity pattern are stored for use during runtime. The following subsections describe the pruning method and quantization procedure in detail.

3.2.1 N:M Pruning Method

As shown in the middle of Figure 2, each column $W[:, j]$ is partitioned along the K dimension into non-overlapping windows of length M_{group}. In each window, we keep the N_{keep} weights with the largest magnitudes and set the remaining $M_{\text{group}} - N_{\text{keep}}$ entries to zero. This simple magnitude-based rule covers common patterns such as 2:4 and generalizes to 2:8, 4:16, and other N:M configurations. The parameters must satisfy

$$0 < N_{\text{keep}} < M_{\text{group}} \leq K \quad \text{and} \quad M_{\text{group}} \mid K.$$

Figure 2: Structured pruning and quantization of the weight matrix. Left: dense FP16 weights before pruning and quantization; purple cells indicate FP16 values. Middle: weights after 2:4 pruning (two nonzeros per group of four along K); white cells indicate zeros. Right: the same pruned pattern after quantization; blue cells indicate INT4 nonzeros.

Pruning is performed once offline on pretrained weights, and the resulting sparse matrices preserve the original dense layout with zeros stored in place. This avoids any additional indexing structure when the weights are later dequantized and consumed by the hardware.

3.2.2 Quantization Method

After pruning, we quantize only the surviving nonzero weights, as illustrated in the right panel of Figure 2, where the remaining FP16 values (purple) are mapped to low-bit integers (blue). We use symmetric abs-max calibration with a global scale and zero-point $z_w = 0$. For a target bit-width b, we define $Q_{\max} = 2^{b-1} - 1$ and compute the scaling factor s by using

$$s = \frac{Q_{\max}}{\max(|W|)}, \tag{1}$$

where the maximum is taken over the pruned weight tensor.

Each floating-point weight w is quantized by

$$q_w = \mathrm{round}(s \cdot w), \tag{2}$$

and the result is clamped to the signed integer range

$$q_w \leftarrow \mathrm{clip}\big(q_w,\, -(Q_{\max} + 1),\, Q_{\max}\big). \tag{3}$$

During runtime, the dequantized FP16 approximation is reconstructed by

$$\hat{w} = \frac{q_w}{s}. \tag{4}$$

In all experiments we use $b = 4$ (INT4) for weights, consistent with the visual representation in Figure 2, while activations remain in FP16.

3.3 Benchmark Execution

In the benchmark execution stage shown on the right side of Figure 1, the pre-compressed weights are consumed by the runtime on each hardware platform. Step ① loads the weights and scaling factors into device memory. Step ② performs dequantization, where the INT4 nonzeros are multiplied by their corresponding scaling factors to reconstruct FP16 values in their original locations, while pruned entries remain zeros. This produces an $M \times K$ sparse FP16 matrix that matches the 2:4 pattern. Finally, Step ③ executes matrix multiplication between the dequantized FP16 weights and the FP16 activation matrix. The resulting $M \times B$ output matrix is fully dense, as shown in the bottom right of Figure 1.

To provide a fair and consistent baseline for our hardware design, we execute the same component-level operation on three software backends, including CPU, dense GPU, and the GPU 2:4 semi-structured kernel, and compare them with our FPGA accelerator. This setup allows us to quantify computational efficiency and memory reduction achieved by the joint pruning and quantization scheme while ensuring that all platforms follow the same execution flow.

CPU Computation On the CPU path, we first reconstruct the dense weights by dequantizing the loaded integers using the stored scaling factor s according to formula 4. The dequantized tensor $\hat{W}$ is cast to floating point and made contiguous in memory. We then compute $C = \hat{W}A$ using PyTorch's CPU Basic Linear Algebra Subprograms (BLAS) backend.

GPU Dense On the GPU path, we mirror the CPU flow but perform dequantization on Compute Unified Device Architecture (CUDA). The resulting floating-point $\hat{W}$ is passed directly to CUDA Basic Linear Algebra Subprograms (cuBLAS) for a standard General Matrix Multiplication (GEMM) with the current activations.

GPU 2:4 Semi-Structured For the sparse path, we convert the floating-point matrix $\hat{W}$ to NVIDIA's semi-structured 2:4 format via `to_sparse_semi_structured`. The resulting sparse handle is then multiplied with activations using CUDA Sparse Library extension for Tensor Cores (cuSPARSELt)'s specialized 2:4 kernel.

3.4 Measurement Methodology

We benchmark the component end-to-end from input files to outputs, with explicit control over I/O and setup costs. The weight matrix $W \in \mathbb{R}^{M\times K}$ is read in from the offline preparation mentioned in 3.2, and the activation matrix $A \in \mathbb{R}^{K\times B}$ with batch size notated as B is generated randomly.

Recorded timings For each benchmark, we record

$$t_{\text{io}}, \quad t_{\text{deq}}, \quad t_{\text{mm}}, \quad t_{\text{compute}},$$

where t_{io} is the time to load the quantized weights and scale, t_{deq} is on-device dequantization to $\hat{W}$ using Eq. 4, t_{mm} is matrix multiplication, and t_{compute} is the compute-only pipeline time, which is from dequant to finished matrix multiplication.

Throughput metric We convert times to GFLOP/s using the dense GEMM count

$$\text{FLOPs}_{\text{dense}} \;=\; 2\,MKB, \qquad \text{GFLOP/s} \;=\; \frac{2\,MKB}{t} \times 10^{-9}, \tag{5}$$

We report throughput for pure matrix multiplication time, and pipeline with/without setup.

Batch size Table 1 compares matrix multiplication time and throughput at batch sizes 1 and 512. Larger batches amortize the kernel launch time and metadata overheads, so the GPU 2:4 sparse kernel shows the expected speedup at $B = 512$. At $B = 1$, however, the overhead of handling sparsity metadata dominates, making the sparse kernel slower than the dense GPU. To highlight the performance where pruning helps, we adopt **batch size** $B = 512$ for all subsequent experiments.

Table 1: Matrix Multiplication time and throughput for different batch sizes across backends

Backend	Batch size	t_{mm} (ms)	$Throughput$mm (GFLOP/s)
CPU	1	2.66	18.85
GPU	1	0.11	295.95
GPU (2:4)	1	0.18	184.58
FPGA (ours)	1	—	
CPU	512	24.66	696.64
GPU	512	0.36	47862.12
GPU (2:4)	512	0.21	81968.13
FPGA (ours)	512	—	

Setup time policy Setup time aggregates costs that are not representative of steady state per-layer execution in large models, including I/O (t_{io}) and the one-time GPU conversion to the 2:4 semi-structured format (t_{conv}, via `to_sparse_semi_structured`). Including these in per-iter totals would dominate the pipeline (Table 2) while not reflecting the target deployment. Therefore, unless otherwise noted, we exclude setup time from steady-state comparisons and report it separately.

Table 2: I/O and compute times across backends

Backend	t_{io} (ms)	t_{compute} (ms)	Throughput (GF/s)
CPU	910	35.38	18.17
GPU	925	0.66	18.56
GPU (2:4)	879	0.51	15.01
FPGA (ours)	1012	—	

Note: Throughput shown for the whole pipeline.

4 Accelerator Design

This section describes the architecture of our FPGA accelerator and how it is co-designed with the N:M sparse, low-bit quantized pipeline introduced in Section 3.1. The goal is to execute the same matrix multiplication $C_{B\times M} = A_{B\times K}W_{K\times M}$ while exploiting weight sparsity to reduce arithmetic operations and matching the available memory bandwidth on the AMD Alveo U55C platform. The accelerator is controlled by a host program running on an Intel Core i9-12900K CPU and is integrated into the same benchmarking framework that we use for the CPU and GPU baselines. The hardware and software platform configuration is summarized in Table 3.

Table 3: Host and FPGA Setup

Accelerator		Host	
Platform	AMD Alevo U55C	CPU	Intel Core i9-12900K
Memory	16GB HBM	RAM	128GB DDR4
XRT	2.18.179	GPU	Nvidia RTX3090
Vitis	2024.2	OpenCL	2.2
Vivado	2024.2	OS	Ubuntu 20.04.6

4.1 Host-Side Processing Pipeline

4.1.1 Dequantization

On the host, we convert the pruned and quantized weights produced by the offline pipeline into the floating-point format used by the accelerator. For each weight matrix, the host reads the INT4 values q_w together with the corresponding scaling factor s (Section 3.2.2) and applies Equation 4. In practice, we avoid per-element division by rewriting the dequantization as a multiplication. Therefore, we precompute the reciprocal α^{-1} once on the host and use

$$w = q_w \cdot \alpha^{-1}.$$

This implementation is friendly to vectorized CPU instructions, which prefers multiplication over division.

4.2 Kernel Design and Optimization

As shown in Figure 3, the systolic array [15] is organized as a 2D grid of processing elements (PEs) fed by on-chip buffers. Tiles of matrix A are first staged in the *Matrix A Buffer* and streamed row-wise through the *Data FIFO*, while tiles of matrix B are stored in the *Matrix B Weight Buffer* and streamed column-wise through the *Weight FIFO*. Each PE receives an activation from its left neighbor and a weight from its upper neighbor, updates its local partial sum, and then forwards the operands to the next PE in the row or column. The resulting outputs are collected in the *Output Buffer*. This streaming dataflow architecture maximizes data reuse within the PE grid, minimizes accesses to off-chip memory, and maintains a regular, high-throughput compute pattern.

4.2.1 Zero-Skipping Processing

Figure 4 shows the microarchitecture of a single PE. Each PE receives a stream of activations and a stream of deqauntized weights. Internally, the PE contains, input registers for the current activation a and weight w, a comparator that checks whether $w = 0$, and an accumulator register that stores the running partial sum. On every cycle, the PR wither performs a multiply-accumulate operation or skips the multiply when the weight is detected zero:

$$\text{if } w \neq 0 \quad \Rightarrow \quad \text{acc} \leftarrow \text{acc} + aw.$$

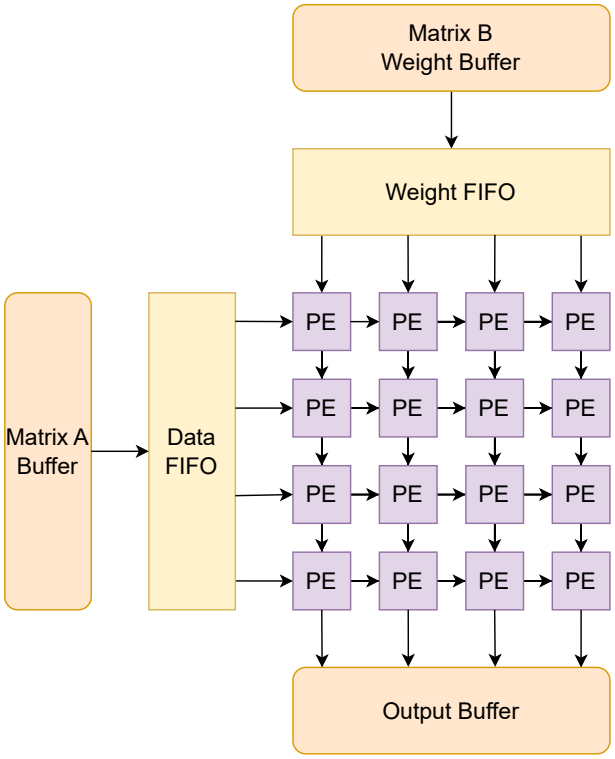

Figure 3: Top-level dataflow of the output-stationary systolic array, showing on-chip buffers and FIFOs that stream tiles of matrix A and matrix B into the PE grid and collect the resulting outputs.

N:M structured sparsity is naturally exploited at the PE level. Because our software pipeline stores pruned weights in a dense layout, whcih means zeros preserved in place, the accelerator does not require explicit sparsity metadata for reconstruction. Instead, each PE inspects the incoming dequantized weight; if $w = 0$, the PE simply forwards the activation and weight to its neighbors without updating the accumulator. When $w \neq 0$, the PE performs a standard floating-point MAC. In a 2:4 pattern, this zero-skipping reduces the number of effective MAC operations by roughly 50% while keeping the PE datapath simple, which no integer arithmetic or scaling factors are needed in hardware.

5 Experimental Results and Evaluation

We run all software and hardware experiments on the same host platform described in Table 3, using an Intel Core i9-12900K CPU and an NVIDIA RTX 3090 GPU together with an AMD Alveo U55C FPGA card.

5.1 Weight Size

We quantify storage under $M = N = 4096$ with FP16 as the baseline and compare the weight sizes after 2:4 pruning and INT4 quantization (Table 4). Pruning to 2 nonzeros per 4 yields 50% density. In our prototype, we store pruned weights in a dense layout (zeros kept in place), so no explicit sparsity metadata is required for persistence or for reconstructing $\hat{W}$ before compute. After quantization, if values are bit-packed to 4 bits, the effective footprint is 8.00 MB plus a negligible global scale ≈ 2 bytes. For simplicity, our current implementation stores the quantized weights as an 8-bit integer tensor, which occupies 16.00 MB again with a ≈ 2 bytes global scale.

In summary, 2:4 pruning halves the FP16 footprint, and adding INT4 quantization yields up to a $4\times$ reduction versus dense FP16 when weights are bit-packed.

5.2 Inference Latency and Throughput

Table 5 reports end-to-end component latency, which is from dequantization to completion of matrix–matrix multiplication, and the corresponding throughput under $M = N = 4096$ and $B = 512$. As expected, the GPU paths outperform

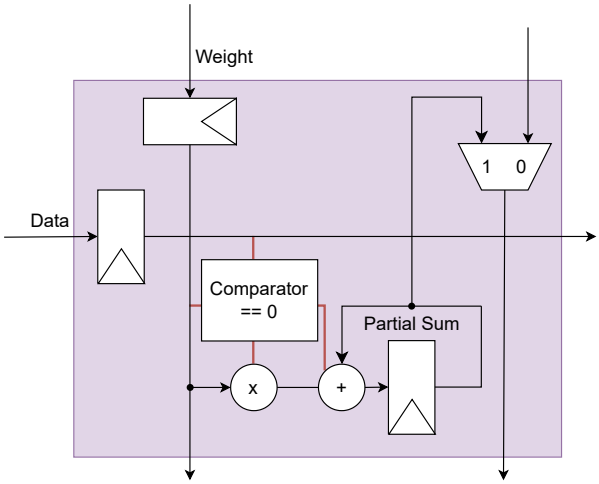

Figure 4: Microarchitecture of a single PE with zero-skipping. Incoming activations (Data) and weights are first latched in input registers (triangular blocks), then passed to a comparator that checks whether the weight is zero. If the weight is nonzero, the PE performs a MAC operation and updates the partial-sum register; otherwise, the multiplier is bypassed and only the registered operands are forwarded to neighboring PEs.

Table 4: Weight size under different schemes for 4096×4096 (2:4 pruning, INT4).

Method / Storage	Relative to dense	Size (MB)
Dense FP16 (no pruning)	$1.00\times$	32.00
Pruned FP16 (nonzeros only, 50% density)	$0.50\times$	16.00
Pruned + Quant INT4 (stored as int tensor)	$0.50\times$	16.00
Pruned + Quant INT4 (bit-packed)	$0.25\times$	8.00

the CPU on both dequantization and GEMM. The 2:4 sparse kernel further reduces GEMM time from 0.36 ms (dense) to 0.21 ms (sparse), a $1.71\times$ speedup, and improves compute-only pipeline time from 0.66 ms to 0.51 ms, a $1.29\times$ speedup. These results indicate that, with greater sparsity, the overall computation time can be reduced.

Table 5: Inference latency and throughput across devices ($M = N = 4096$, $B = 512$)

Backend	t_{dequant} (ms)	t_{mm} (ms)	t_{compute} (ms)	$Throughput_{\text{mm}}$ (GFLOP/s)	$Throughput_{\text{compute}}$ (GFLOP/s)
CPU	10.72	24.66	35.38	696.64	485.53
GPU	0.30	0.36	0.66	47862.12	25928.91
GPU (2:4)	0.32	0.21	0.51	81968.13	32690.74
FPGA (ours)				—	

5.3 Effect of Matrix Size

We evaluate how performance scales as the matrix size grows, and the results are given in Table 6. As M and N grow, arithmetic intensity and GPU occupancy improve, so GPU throughput rises while CPU remains an order of magnitude lower. The 2:4 sparse kernel consistently outperforms dense GPU on GEMM and the compute-only pipeline once metadata costs are amortized. GEMM time drops from $0.36 \rightarrow 0.21$ ms at 4096×4096 ($1.71\times$), $1.05 \rightarrow 0.64$ ms at 8192×8192 ($1.64\times$), and $2.26 \rightarrow 1.16$ ms at 12288×12288 ($1.95\times$). End-to-end compute time (dequant+GEMM) also improves with sparsity, $0.66 \rightarrow 0.51$ ms ($1.29\times$), $1.77 \rightarrow 1.38$ ms ($1.28\times$), and $3.70 \rightarrow 2.59$ ms ($1.43\times$), indicating that larger problems more effectively hide metadata handling and highlight the benefit of structured pruning.

5.4 Predicted Results for LLaMA-7B

We estimate the per-token compute cost contributed by the linear layers of LLaMA-7B in order to measure the feasibility of our approach at model scale. LLaMA-7B has $L = 32$ decoder blocks. Each block contains four attention projections

Table 6: Latency and throughput at different matrix sizes

		Time (ms)			Throughput (GFLOP/s)	
Backend	(M, N)	Dequant	GEMM	Compute	GEMM	Compute
CPU	(4096, 4096)	10.72	24.66	35.38	696.64	485.53
GPU	(4096, 4096)	0.30	0.36	0.66	47 862.12	25 928.91
GPU (2:4)	(4096, 4096)	0.32	0.21	0.51	81 968.13	32 690.74
FPGA (ours)	(4096, 4096)				—	
CPU	(8192, 8192)	42.33	88.90	131.22	773.01	523.67
GPU	(8192, 8192)	0.75	1.05	1.77	65 267.91	38 871.23
GPU (2:4)	(8192, 8192)	0.74	0.64	1.38	106 728.13	48 470.63
FPGA (ours)	(8192, 8192)				—	
CPU	(12288, 12288)	95.00	203.40	298.40	760.18	518.16
GPU	(12288, 12288)	1.43	2.26	3.70	68 379.14	41 877.19
GPU (2:4)	(12288, 12288)	1.42	1.16	2.59	132 745.67	59 766.85
FPGA (ours)	(12288, 12288)				—	

Q, K, V, and O with weight shapes 4096×4096. The MLP uses two up paths of shape 4096×11008 and one down path of shape 11008×4096.

Let $T_{\text{linear}}(M, N, B)$ denote the compute time, defined as dequantization plus GEMM, for a linear layer with weight $M\times N$ and batch B. The per-block compute time at batch B is

$$T_{\text{block}}(B) = 4\times T_{\text{linear}}(4096, 4096, B) + 2\times T_{\text{linear}}(4096, 11008, B) + 1\times T_{\text{linear}}(11008, 4096, B). \tag{6}$$

From Table 5 we obtain $T_{\text{linear}}(4096, 4096, 512)$, and from Table 7 we obtain $T_{\text{linear}}(4096, 11008, 512)$. We do not directly measure $T_{\text{linear}}(11008, 4096, 512)$; since FLOPs and memory traffic are comparable, we approximate it by $T_{\text{linear}}(4096, 11008, 512)$.

GPU (2:4 sparse)

$$t_{\text{comp}}^{4096\times4096} = 0.51 \text{ ms}, \quad t_{\text{comp}}^{4096\times11008} = 0.97 \text{ ms}.$$
$$T_{\text{block}}^{\text{sparse}}(512) \approx 4\times(0.51) + 2\times(0.97) + 1\times(0.97) = 4.95 \text{ ms}.$$

GPU

$$t_{\text{comp}}^{4096\times4096} = 0.66 \text{ ms}, \quad t_{\text{comp}}^{4096\times11008} = 1.36 \text{ ms}.$$
$$T_{\text{block}}^{\text{dense}}(512) \approx 4\times(0.66) + 2\times(1.36) + 1\times(1.36) = 6.72 \text{ ms}.$$

CPU

$$t_{\text{comp}}^{4096\times4096} = 35.38 \text{ ms}, \quad t_{\text{comp}}^{4096\times11008} = 94.45 \text{ ms}.$$
$$T_{\text{block}}^{\text{cpu}}(512) \approx 4\times(35.38) + 2\times(94.45) + 1\times(94.45) = 424.9 \text{ ms}.$$

The predicted model latency is $T_{\text{model}}(B) = L \cdot T_{\text{block}}(B)$ with $L = 32$. The corresponding model-level throughput is $F_{\text{model}}/T_{\text{model}}$, where the per-block FLOPs for linear layers is

$$F_{\text{block}} = 4 \cdot 2 \cdot 4096^2 \cdot B \ + \ 3 \cdot 2 \cdot 4096 \cdot 11008 \cdot B = 2.072 \times 10^{11} \text{ FLOPs} \quad \text{for } B = 512,$$

and $F_{\text{model}} = L \cdot F_{\text{block}} = 6.631 \times 10^{12}$ FLOPs. The results of the predicted latency and throughput for LLaMA-7B is shown in Table 8. Under this model prediction with $B = 512$, the 2:4 sparse GPU path predicts a $1.36\times$ speedup over dense GPU and $85.67\times$ speedup over CPU.

These predictions include only dequantization and matrix multiplication for the linear layers. They exclude attention score computation, softmax, rotary embeddings, residual adds, normalizations, cache reads and writes, and embedding or head layers. They also assume steady execution with setup costs excluded. In practice, overall token latency will be higher once the omitted components are included, but the relative advantage of structured sparsity should remain similar. Finally, our hardware targets general $N : M$ patterns, with higher sparsity such as $4 : 16$ would further reduce FLOPs and memory traffic, potentially yielding larger gains than the 2:4 results shown here.

Table 7: Inference latency and throughput across devices ($M = 4096$, $N = 11008$, $B = 512$)

Backend	t_{dequant} (ms)	t_{mm} (ms)	t_{compute} (ms)	$Throughput_{\text{mm}}$ (GFLOP/s)	$Throughput_{\text{compute}}$ (GFLOP/s)
CPU	30.60	63.84	94.45	723.21	488.86
GPU	0.52	0.84	1.36	54964.57	33843.08
GPU (2:4)	0.52	0.45	0.97	103132.10	47595.38
FPGA (ours)			—		

Table 8: Predicted latency and throughput for LLaMA-7B linear layers only ($L = 32$ blocks, $B = 512$).

Backend	T_{block} (ms)	T_{model} (ms)	$\text{Throughput}_{\text{model}}$ (GFLOP/s)
CPU	424.90	13596.80	488
GPU	6.72	215.04	30838
GPU (2:4)	4.95	158.40	41865
FPGA (ours)		—	

Note: FLOPs per block (linear layers only): $F_{\text{block}} = 4 \cdot 2 \cdot 4096^2 \cdot 512 + 3 \cdot 2 \cdot 4096 \cdot 11008 \cdot 512 = 2.072 \times 10^{11}$. Total per model: $F_{\text{model}} = 32 \cdot F_{\text{block}} = 6.631 \times 10^{12}$. Throughput is $F_{\text{model}}/T_{\text{model}}$.

6 Conclusion

This work presented an FPGA-software co-design framework that combines N:M structured pruning with low-bit quantization to accelerate large language model inference. By unifying offline N:M pruning, INT4 weight quantization, host-side dequantization, and a zero-skipping systolic array, our pipeline jointly reduces weight storage, memory traffic, and arithmetic cost while keeping a single compressed representation that can be executed on CPU, GPU, and FPGA backends.

On synthetic 4096×4096 workloads with 2:4 sparsity and INT4 weights, our scheme achieves up to a $4\times$ reduction in effective weight footprint with bit-packing and delivers a $1.71\times$ GEMM speedup and $1.29\times$ end-to-end compute gain over dense GPU baselines. A scaling analysis on the linear layers of LLaMA-7B further suggests that structured sparsity can improve predicted per-token throughput by $1.36\times$ compared with dense execution, indicating that the benefits of N:M pruning and quantization persist at model scale.

Our FPGA accelerator is designed to support general N:M patterns beyond the fixed 2:4 configuration available on current GPUs, providing a path toward more flexible sparsity-aware hardware. As future work, we plan to complete a full empirical evaluation of the FPGA implementation, including power and energy efficiency, extend the framework from component-level kernels to end-to-end LLaMA inference, and explore richer sparsity and quantization schemes, such as higher-ratio N:M patterns and mixed-precision activations, to further reduce the cost of large-model deployment on edge and datacenter platforms.

References

[1] T. Brown, B. Mann, N. Ryder, M. Subbiah, J. D. Kaplan, P. Dhariwal, A. Neelakantan, P. Shyam, G. Sastry, A. Askell, S. Agarwal, A. Herbert-Voss, G. Krueger, T. Henighan, R. Child, A. Ramesh, D. Ziegler, J. Wu, C. Winter, C. Hesse, M. Chen, E. Sigler, M. Litwin, S. Gray, B. Chess, J. Clark, C. Berner, S. McCandlish, A. Radford, I. Sutskever, and D. Amodei, "Language models are few-shot learners," in *Advances in Neural Information Processing Systems*, H. Larochelle, M. Ranzato, R. Hadsell, M. Balcan, and H. Lin, Eds., vol. 33. Curran Associates, Inc., 2020, pp. 1877–1901. [Online]. Available: https://proceedings.neurips.cc/paper_files/paper/2020/file/1457c0d6bfcb4967418bfb8ac142f64a-Paper.pdf

[2] M. Mozaffari, A. Yazdanbakhsh, and M. M. Dehnavi, "SLim: One-shot quantization and sparsity with low-rank approximation for LLM weight compression," in *Forty-second International Conference on Machine Learning*, 2025. [Online]. Available: https://openreview.net/forum?id=4UfRP8MopP

[3] E. Frantar and D. Alistarh, "Sparsegpt: massive language models can be accurately pruned in one-shot," in *Proceedings of the 40th International Conference on Machine Learning*, ser. ICML'23. JMLR.org, 2023.

[4] A. Gholami, S. Kim, Z. Dong, Z. Yao, M. W. Mahoney, and K. Keutzer, "A survey of quantization methods for efficient neural network inference," 2021. [Online]. Available: https://arxiv.org/abs/2103.13630

[5] J. Guo, J. Wu, Z. Wang, J. Liu, G. Yang, Y. Ding, R. Gong, H. Qin, and X. Liu, "Compressing large language models by joint sparsification and quantization," in *Forty-first International Conference on Machine Learning*, 2024. [Online]. Available: https://openreview.net/forum?id=sCGRhnuMUJ

[6] M. Zhu and S. Gupta, "To prune, or not to prune: exploring the efficacy of pruning for model compression," 2017. [Online]. Available: https://arxiv.org/abs/1710.01878

[7] I. Hubara, M. Courbariaux, D. Soudry, R. El-Yaniv, and Y. Bengio, "Quantized neural networks: training neural networks with low precision weights and activations," *J. Mach. Learn. Res.*, vol. 18, no. 1, p. 6869–6898, Jan. 2017.

[8] Z. Zhou, X. Ning, K. Hong, T. Fu, J. Xu, S. Li, Y. Lou, L. Wang, Z. Yuan, X. Li, S. Yan, G. Dai, X.-P. Zhang, Y. Dong, and Y. Wang, "A survey on efficient inference for large language models," *ArXiv*, vol. abs/2404.14294, 2024. [Online]. Available: https://api.semanticscholar.org/CorpusID:269293007

[9] T. Sharma, M. Ali, I. Chakraborty, and K. Roy, "Www: What, when, where to compute-in-memory," 2025. [Online]. Available: https://arxiv.org/abs/2312.15896

[10] Y. He and L. Xiao, "Structured pruning for deep convolutional neural networks: A survey," *IEEE Transactions on Pattern Analysis and Machine Intelligence*, vol. 46, no. 5, p. 2900–2919, May 2024. [Online]. Available: http://dx.doi.org/10.1109/TPAMI.2023.3334614

[11] S. Han, H. Mao, and W. J. Dally, "Deep compression: Compressing deep neural networks with pruning, trained quantization and huffman coding," 2016. [Online]. Available: https://arxiv.org/abs/1510.00149

[12] T. Dettmers, R. Svirschevski, V. Egiazarian, D. Kuznedelev, E. Frantar, S. Ashkboos, A. Borzunov, T. Hoefler, and D. Alistarh, "Spqr: A sparse-quantized representation for near-lossless llm weight compression," 2023.

[13] S. Kim, C. Hooper, A. Gholami, Z. Dong, X. Li, S. Shen, M. W. Mahoney, and K. Keutzer, "Squeezellm: dense-and-sparse quantization," in *Proceedings of the 41st International Conference on Machine Learning*, ser. ICML'24. JMLR.org, 2024.

[14] J. Guo, J. Wu, Z. Wang, J. Liu, G. Yang, Y. Ding, R. Gong, H. Qin, and X. Liu, "Compressing large language models by joint sparsification and quantization," in *Forty-first International Conference on Machine Learning*, 2024. [Online]. Available: https://openreview.net/forum?id=sCGRhnuMUJ

[15] H. T. Kung and C. E. Leiserson, "Systolic Arrays for (VLSI)," Carnegie-Mellon University, Department of Computer Science, Pittsburgh, PA, Tech. Rep. 79/103, 1978.

Author Biographies

Fen-Yu Hsieh received the BS degree in computer science from National Tsing Hua University in 2025. She is currently a research assistant at the Institute of Information Science, Academia Sinica. Her research interests include computer architecture, model compression, N:M structured sparsity, low-bit quantization, hardware/software co-design, and accelerator support for efficient large language model inference on GPUs and FPGAs. In this paper, she conceived the overall compression–acceleration framework, designed the N:M sparsity and quantization pipeline, implemented the CPU and dense/sparse GPU baselines and benchmarking scripts, developed the measurement methodology and LLaMA-7B scaling analysis, and led the writing and revision of the manuscript.

Yun-Chang Teng received his B.S. degree in Computer Engineering from the University of Massachusetts Lowell and M.S. degree from the University of Washington, Seattle in 2023. He is currently a Research Assistant at the Institute of Information Science, Academia Sinica. His research interests span computer architecture/parallel architectures, domain-specific accelerators, digital ASIC/VLSI design, and hardware/software co-design. He developed the systolic array-based accelerator for GEMM, bridged software and hardware by implementing the host to interface with the accelerator and offload workloads, and orchestrated the high-level synthesis and FPGA design flows, and performed power, performance, area analyses and evaluation.

Ding-Yong Hong received the BS, MS, and PhD degrees in computer science from National Tsing Hua University in 2004, 2005, and 2013, respectively. He is currently an associate research fellow at the Institute of Information Science, Academia Sinica. His research interests include compiler optimization, dynamic binary translation, computer architecture, and parallel and distributed computing.

Jan-Jan Wu received the BS and MS degrees in computer science from National Taiwan University in 1985 and 1987, respectively, and the MS and PhD degrees in computer science from Yale University in 1991 and 1995, respectively. She is currently a research fellow and the leader of the Computer Systems Laboratory at the Institute of Information Science, Academia Sinica. Her current research interests include parallel and distributed computing, cloud computing, cloud databases, virtualization, and dynamic binary translation on multicores.